REPORT DOCUMENTATION PAGE

Form Approved
OMB No. 0704-0188

1. AGENCY USE ONLY (Leave blank)	2. REPORT DATE 7/24/95	3. REPORT TYPE AND DATES COVERED Final 1 Jun 92 - 31 May 95

4. TITLE AND SUBTITLE

"On Mechanical Properties of Materials by Thermal Wave Imaging"

5. FUNDING NUMBERS

DAAL03-92-G-0246

6. AUTHOR(S)

R.L. Thomas, L.D. Favro, and P.K. Kuo

7. PERFORMING ORGANIZATION NAME(S) AND ADDRESS(ES)

Institute for Manufacturing Research
Wayne State University
Detroit, Michigan 48202

8. PERFORMING ORGANIZATION REPORT NUMBER

DTIC
SELECTED
OCT 27 1995
F

9. SPONSORING/MONITORING AGENCY NAME(S) AND ADDRESS(ES)

U.S. Army Research Office
P.O. Box 12211
Research Triangle Park, NC 27709-2211

10. SPONSORING/MONITORING AGENCY REPORT NUMBER

ARO 28780.12-MS

11. SUPPLEMENTARY NOTES

The views, opinions and/or findings contained in this report are those of the author(s) and should not be construed as an official Department of the Army position, policy, or decision, unless so designated by other documentation.

12a. DISTRIBUTION/AVAILABILITY STATEMENT

Approved for public release; distribution unlimited.

12b. DISTRIBUTION CODE

13. ABSTRACT (Maximum 200 words)

ABSTRACT FOR ARO FINAL REPORT 7/24/95

Research was carried out to: 1) Utilize WSU fast imaging techniques to study the temperature distribution in the vicinity of the crack tips of propagating cracks in polymer composites; 2) Utilize Wayne State University's thermal wave imaging techniques for studying adhesive bond strength, and 3) Exploit the concept of vector lock-in video thermal wave imaging for mechanical and thermal response of semiconductors. Key results included 1) a Physical Review Letter: "The Thermal conductivity of Isotopically Modified Single Crystal Diamond," Lanhua Wei, P.K. Kuo, R.L. Thomas, T.R. Anthony and W.F. Banholzer, *Phys. Rev. Letters* 70, No. 24, pp. 3764-3767 (14June, 1993); 2) Thermal wave imaging ["Thermal Wave Imaging of the Temperature Distributions around Propagating Cracks in Polymers", R.L. Thomas, L.D. Favro, P.K. Kuo, Z.L. Wu, T. Ahmed, X. Wang, Yingxia Wang, L.C. Jiang, and H. Van Oene Review of Progress in Quantitative NDE, Vol. 13, edited by D.O. Thompson and D. Chimenti, Plenum New York, pp. 1641-1644 (1994).] and analysis [to be published] of crack initiation and propagation in polymers [comparing to the theory of C. Levy and G. Herrmann, *Eng. Fract. Mech.* 17, 125 (1983).]; 3) Thermal wave imaging of fracture in metal/metal adhesive bonds.

14. SUBJECT TERMS

DTIC QUALITY INSPECTED 5

15. NUMBER OF PAGES
20

16. PRICE CODE

17. SECURITY CLASSIFICATION OF REPORT	18. SECURITY CLASSIFICATION OF THIS PAGE	19. SECURITY CLASSIFICATION OF ABSTRACT	20. LIMITATION OF ABSTRACT
UNCLASSIFIED	UNCLASSIFIED	UNCLASSIFIED	UL

NSN 7540-01-280-5500

Standard Form 298 (Rev 2-89)
Prescribed by ANSI Std. Z39-18

19951025 051

ON MECHANICAL PROPERTIES OF MATERIALS BY THERMAL WAVE IMAGING

FINAL REPORT

R.L. THOMAS, L.D. FAVRO AND P.K. KUO

Accesion For		
NTIS CRA&I	☑	
DTIC TAB	☐	
Unannounced	☐	
Justification		
By		
Distribution /		
Availability Codes		
Dist	Avail and / or Special	
A-1		

JULY 24, 1995

U.S. ARMY RESEARCH OFFICE

CONTRACT NUMBER DAAL-03-92-G-0246

WAYNE STATE UNIVERSITY

ON MECHANICAL PROPERTIES OF MATERIALS BY THERMAL WAVE IMAGING

R.L. Thomas, L.D. Favro, and P.K. Kuo, Wayne State University

APPROVED FOR PUBLIC RELEASE;
DISTRIBUTION UNLIMITED.

ON MECHANICAL PROPERTIES OF MATERIALS BY THERMAL WAVE IMAGING
R.L. Thomas, L.D. Favro, and P.K. Kuo, Wayne State University

TABLE OF CONTENTS

ON MECHANICAL PROPERTIES OF MATERIALS BY THERMAL WAVE IMAGING
R.L. Thomas, L.D. Favro, and P.K. Kuo, Wayne State University

LIST OF ILLUSTRATIONS

ON MECHANICAL PROPERTIES OF MATERIALS BY THERMAL WAVE IMAGING
R.L. Thomas, L.D. Favro, and P.K. Kuo, Wayne State University

ACCOMPLISHMENTS UNDER THE CONTRACT

A.   STATEMENT OF THE PROBLEM STUDIED

A three year program of research was proposed to: 1) Utilize recently developed WSU fast line-scan techniques to study the temperature distribution in the vicinity of the crack tips of propagating brittle fracture cracks in structural polymer composites; 2) To utilize Wayne State University's well established box-car video thermal wave imaging technique for the purpose of studying adhesive bond strength, and 3) Exploit the concept of vector lock-in video thermal wave imaging for mechanical and thermal response of semiconductors.

B.   SUMMARY OF THE MOST IMPORTANT RESULTS

1)   The Thermal conductivity of Isotopically Modified Single Crystal Diamond.

A thermal wave materials characterization project in diamond, with ARO support, has led to a fundamental understanding of that material as a heat spreader. Our results were published in a Physical Review Letter: "The Thermal conductivity of Isotopically Modified Single Crystal Diamond," Lanhua Wei, P.K. Kuo, R.L. Thomas, T.R. Anthony and W.F. Banholzer, *Phys. Rev. Letters* 70, No. 24, pp. 3764-3767 (14 June, 1993). This research was the culmination of a collaboration of Wayne State University and General Electric Corporate R&D, in which we found new experimental results on the thermal conductivity of isotopically enriched ^{12}C diamond crystals at low temperatures. To our knowledge, the measured value for a 99.9% ^{12}C crystal at 104K, 410 W/cmK, is the highest measured thermal conductivity for any solid above liquid nitrogen temperature.

Diamond as a material has many outstanding physical properties, one of the most striking of which is its thermal conductivity (5 times that of copper at room temperature). The two stable isotopes of carbon, ^{12}C and ^{13}C, have natural abundances of 98.9% and 1.1%, respectively. It was reported by the authors in 1990 that, by enriching the isotopic purity of ^{12}C from the natural 98.9% to 99.9%, the thermal conductivity of diamond crystals at room temperature is enhanced by nearly 50%. The magnitude of the enhancement is surprising, since in similar systems such as LiF (^{6}Li and ^{7}Li) or He (^{3}He and ^{4}He) the isotopic effect is only 1~2% at the same reduced temperature. The unusual enhancement in the thermal conductivity of diamond at room temperature has since been confirmed by researchers from other laboratories around the country using a variety of techniques. The Wayne State researchers have also reported the dependence of the room temperature thermal conductivity on ^{13}C content over a range from 0.07% to 99% ^{13}C.

In Fig. 1, [from the Phys. Rev. Letter cited above], we summarize the results of fits of our data to
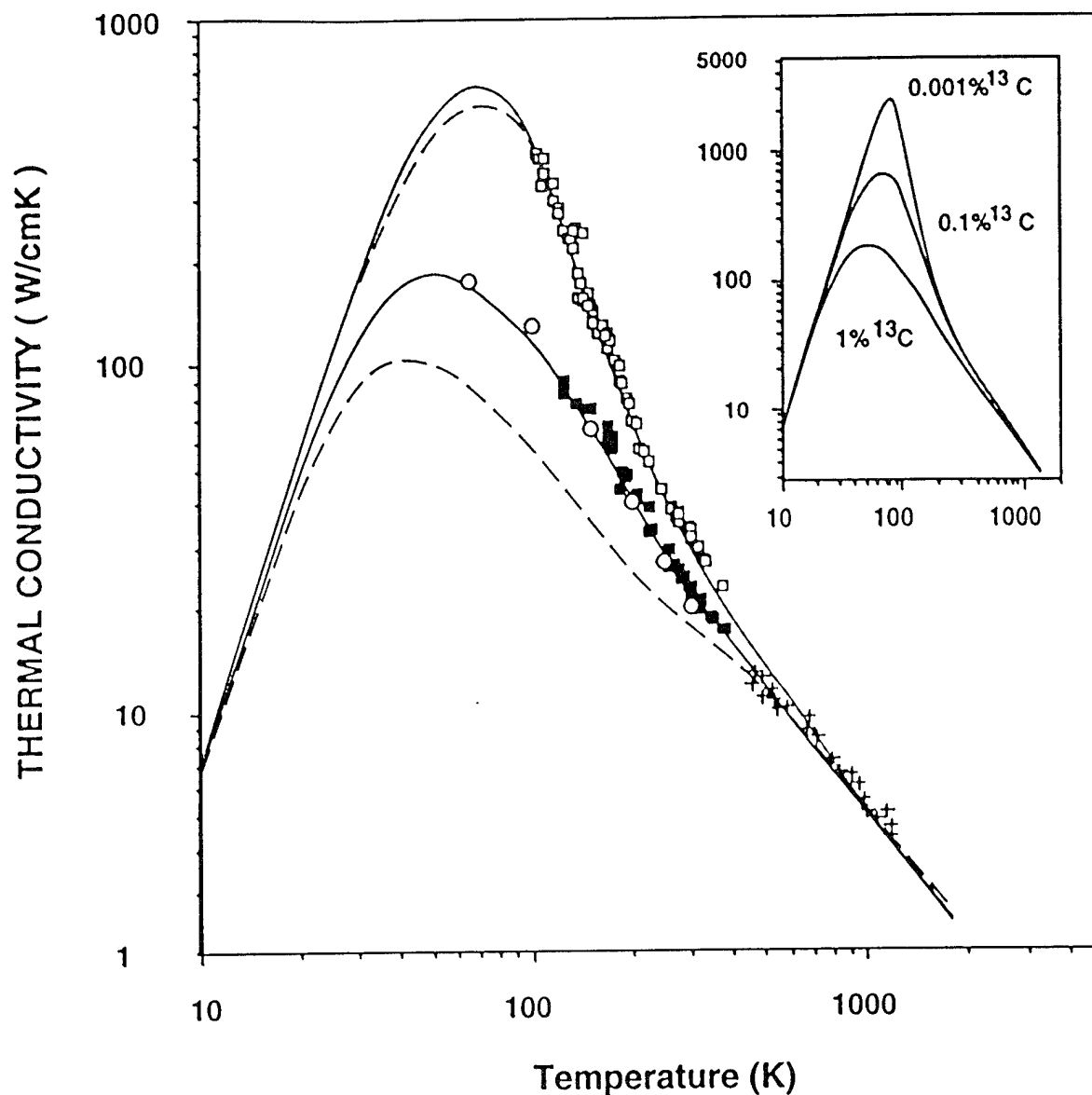
Fig. 1 Thermal conductivity of natural abundance (1.1% ^{13}C) diamond (lower squares), isotopically enriched (0.1% ^{13}C) diamond (upper squares), together with the low temperature data of Slack (circles) and the high temperature data of Olson et al. (crosses). The solid curves are the results of fitting the Callaway theory to the data, using the same set of fitting parameters. The dashed curves are the results of fitting with the assumption that N-processes dominate. The inset shows the calculated thermal conductivity corresponding to 1%, 0.1%, and 0.001% ^{13}C-concentrations according to the Callaway theory.

the full Callaway model, extended to take into account the differences among the longitudinal and transverse phonon modes. In the paper, and as illustrated in Fig. 1, we show that our measured temperature dependent conductivities for the isotopically enriched diamond and natural abundance diamond specimens are well described by Callaway's theoretical model. We predict that the thermal conductivity of

a 99.999% ^{12}C diamond crystal should exceed 2000 W/cmK at ~80K. It is of practical importance that this peak is predicted to occur above liquid nitrogen temperature.

2) Thermal Wave Imaging of the Temperature Distributions around Propagating Cracks in Polymers.

The research project was carried out in collaboration with Dr. Henk Van Oene of Ford Scientific Research Labs. It was aimed at examining the spatial and temporal distribution of energy dissipation in the vicinity of brittle fracture cracks in polymer materials. The technique utilized infrared (IR) cameras, operating in two different spectral bands (3μm - 5μm and 8μm - 12μm) of the IR, and with different image frame rates, ranging from 30 Hz to 244 Hz. A table-top tensile tester was used to apply tensile stress to notched polymer test coupons, using uniform drawing speeds which are varied up to 100 mm/minute (see Fig. 2). During the tensile test, the IR emission from the coupon is monitored as a function of time, using a SantaBarbara 128 x 128 InSb focal plane array camera (3μm - 5μm spectral band/ up to 244 Hz frame rate). By way of illustration, in Fig. 3 we show a set of selected frames from such a tensile test on a coupon of rubber-modified polystyrene, using the Santa Barbara camera at 244 Hz. In Fig. 4, we show one frame taken at the initiation time of a crack in a rubber-modified polystyrene test sample, with a spatial resolution of about 40μm/pixel. It can be seen from Fig. 4, that the position of greatest IR emission in the vicinity of the crack tip can be measured quite precisely as a function of position, with a temporal resolution of about 4 msec (with this camera). Fig. 5 shows a later frame from a similar sequence to that shown in Fig. 2, illustrating a "snapshot" of the IR emission profile in the vicinity of the propagating crack. The general features of the experiment confirm that a material with a positive thermal expansion coefficient cools when it is deformed elastically in tension. In some of our experiments, we utilize the detection of this elastic cooling to trigger the data acquisition which follows. In other cases, we trigger from a simultaneous stress-strain measurement, beginning to record images at the onset of plastic deformation.
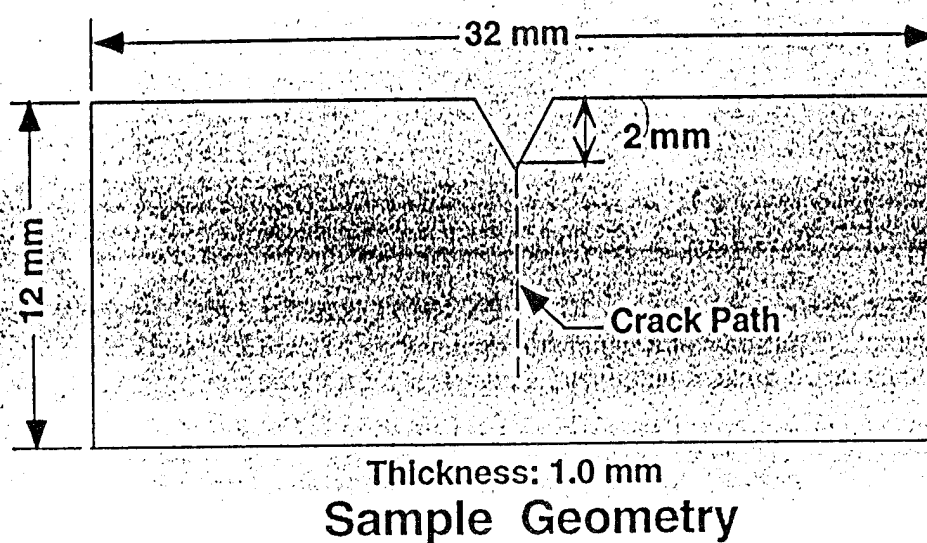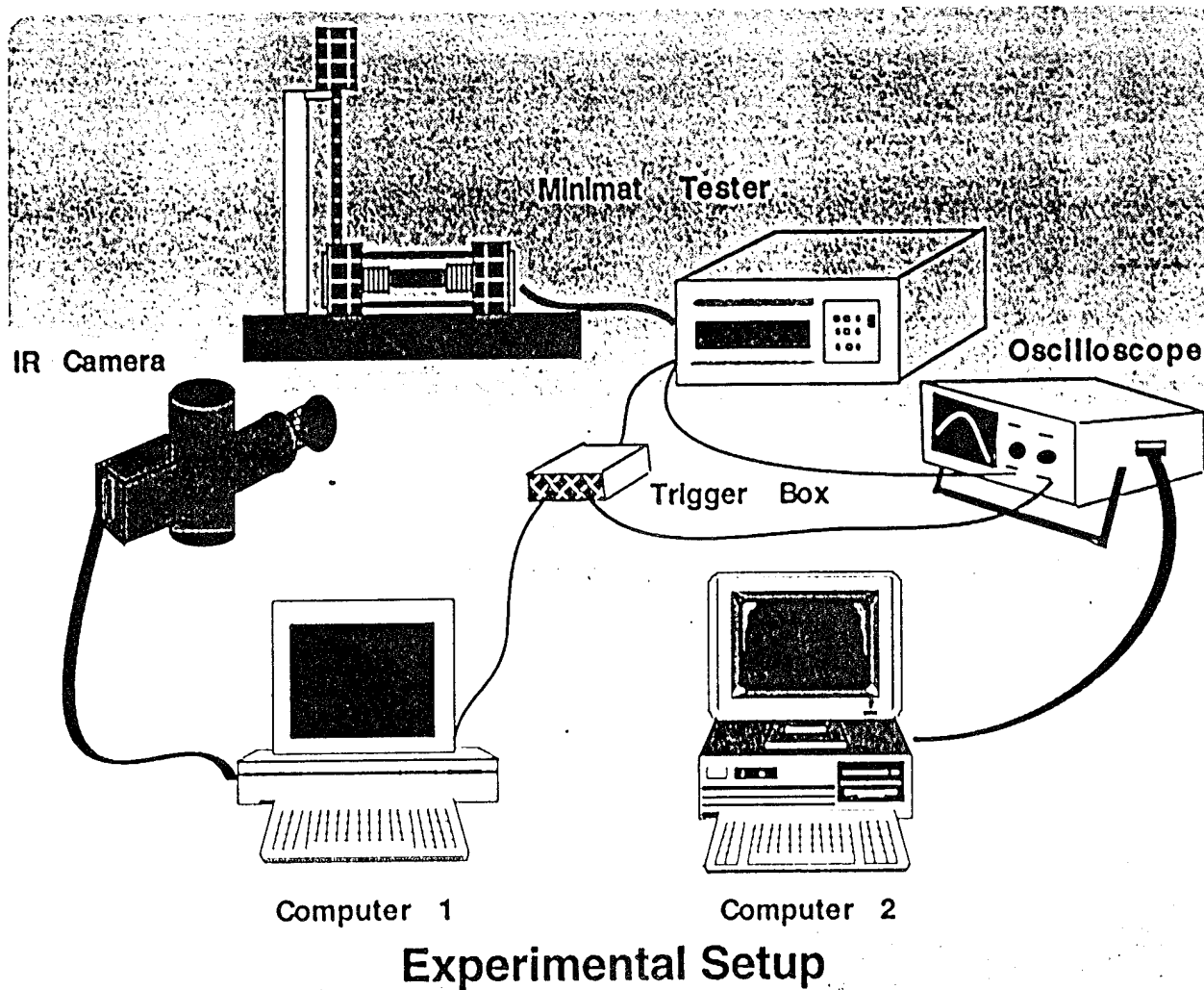
Fig. 2   Experimental setup for acquiring the images shown in Figs. 3 and 4.

Frame #20

Frame #30

Frame #40

Frame #50

Frame #60

Frame #70

Frame #80

Frame #90

Frame #100

Frame rate: 24.4 Hz   5 mm   crosshead speed = 20 mm/min
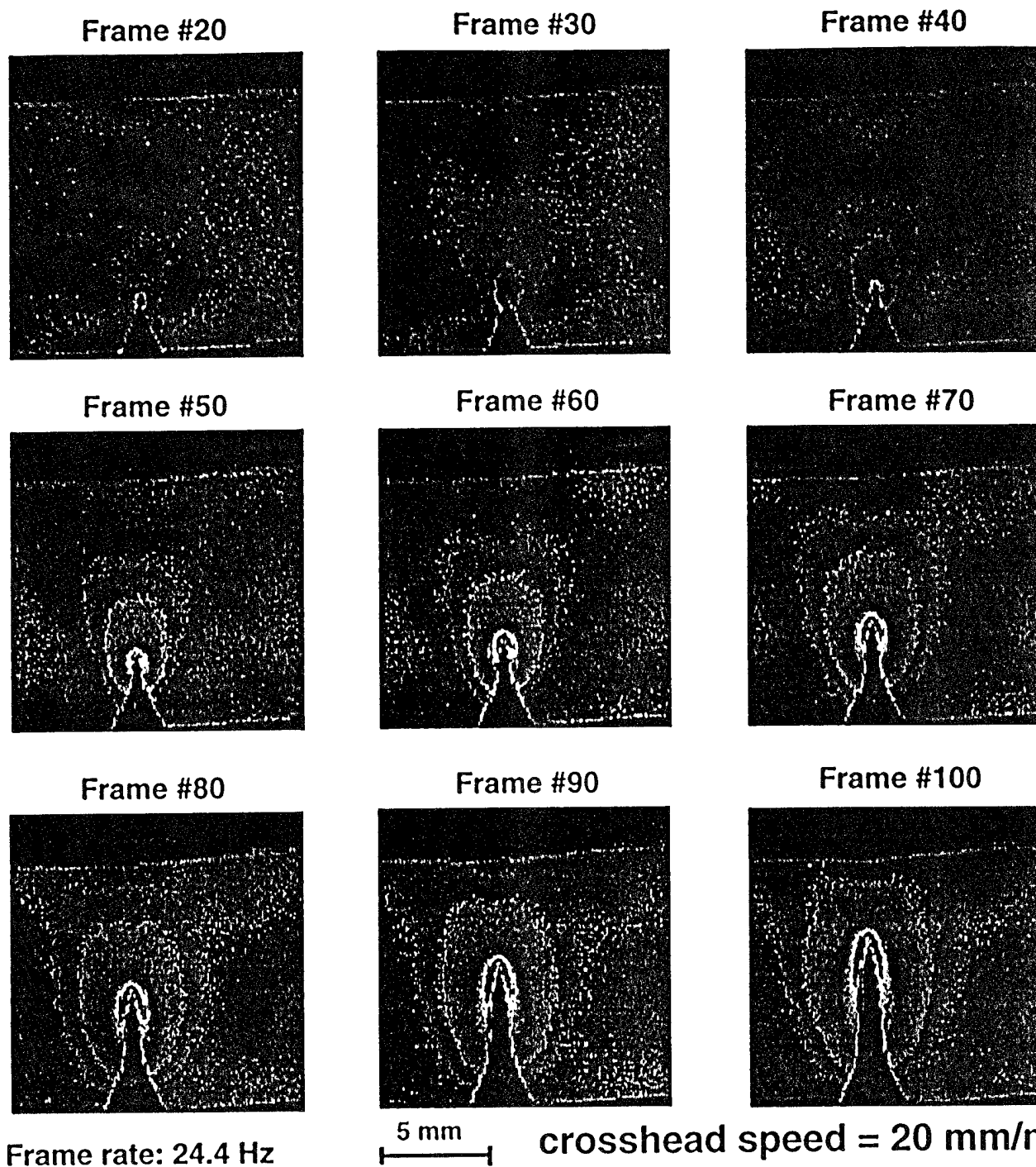
Fig. 3   Sequence of frames taken during the initiation and propagation of a crack in a rubber-modified polystyrene test sample, using the Santa Barbara camera at 244.
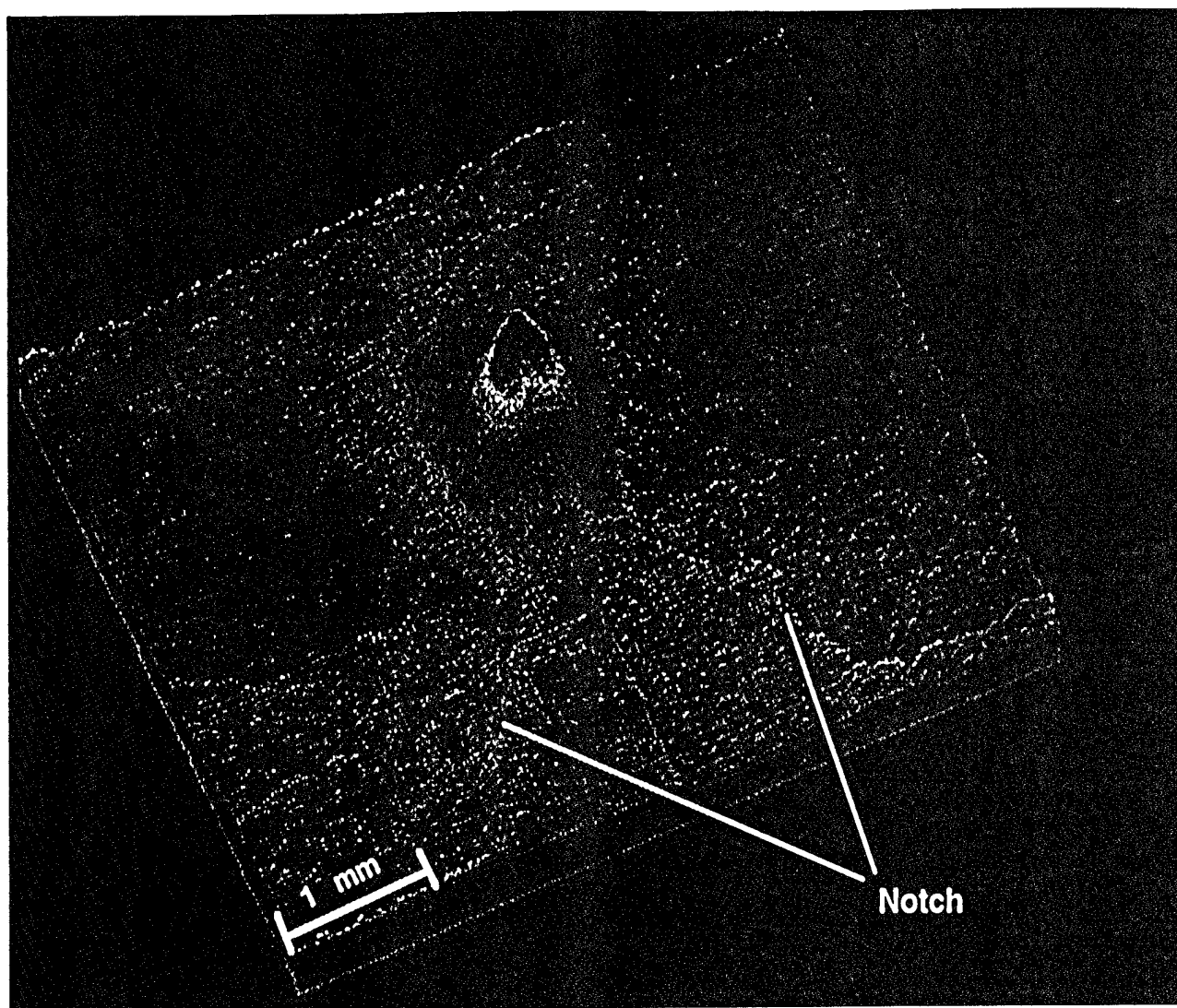
Fig. 4   One frame taken at the initiation time of a crack in a rubber-modified polystyrene test sample, using the Santa Barbara camera at 244 Hz, and with a spatial resolution of about 40μm/pixel.
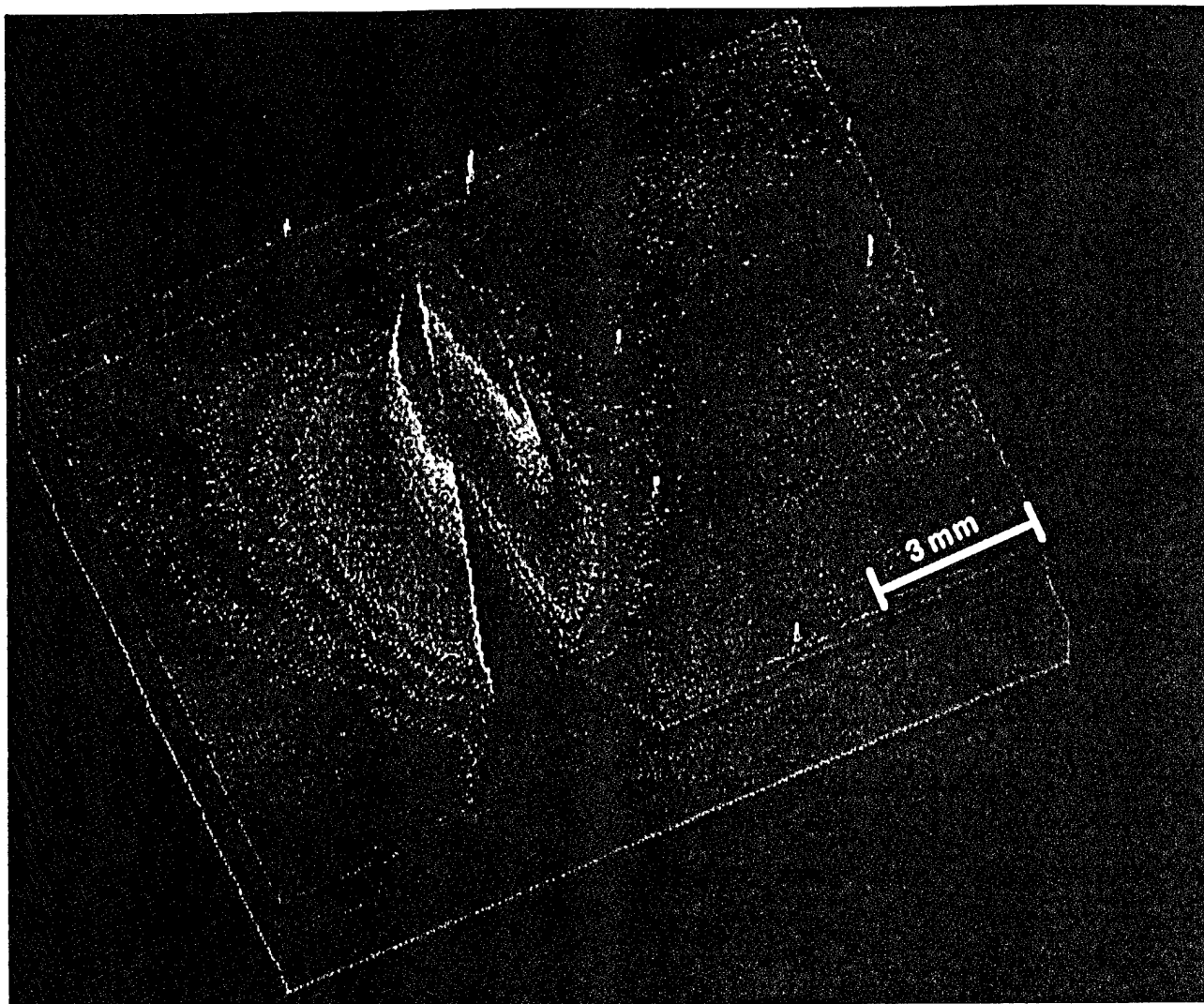
Fig. 5   One frame taken during the propagation time of a crack in a rubber-modified polystyrene test sample, using the Santa Barbara camera at 244 Hz, with a spatial resolution of about 120μm/pixel.

We assume that plastic yielding occurs mostly near the crack tip, so that the location of the crack tip is revealed by the largest observed temperature in the image field. A typical experiment yields about a hundred consecutive images. Hence, a rather dense set of data can be analyzed, both for the initial yielding and crack intiation, and for the subsequent "catastrophic" propagation. An example of the raw data for three samples of high-impact polystyrene, taken at three different pulling speeds, is shown in Fig. 6.
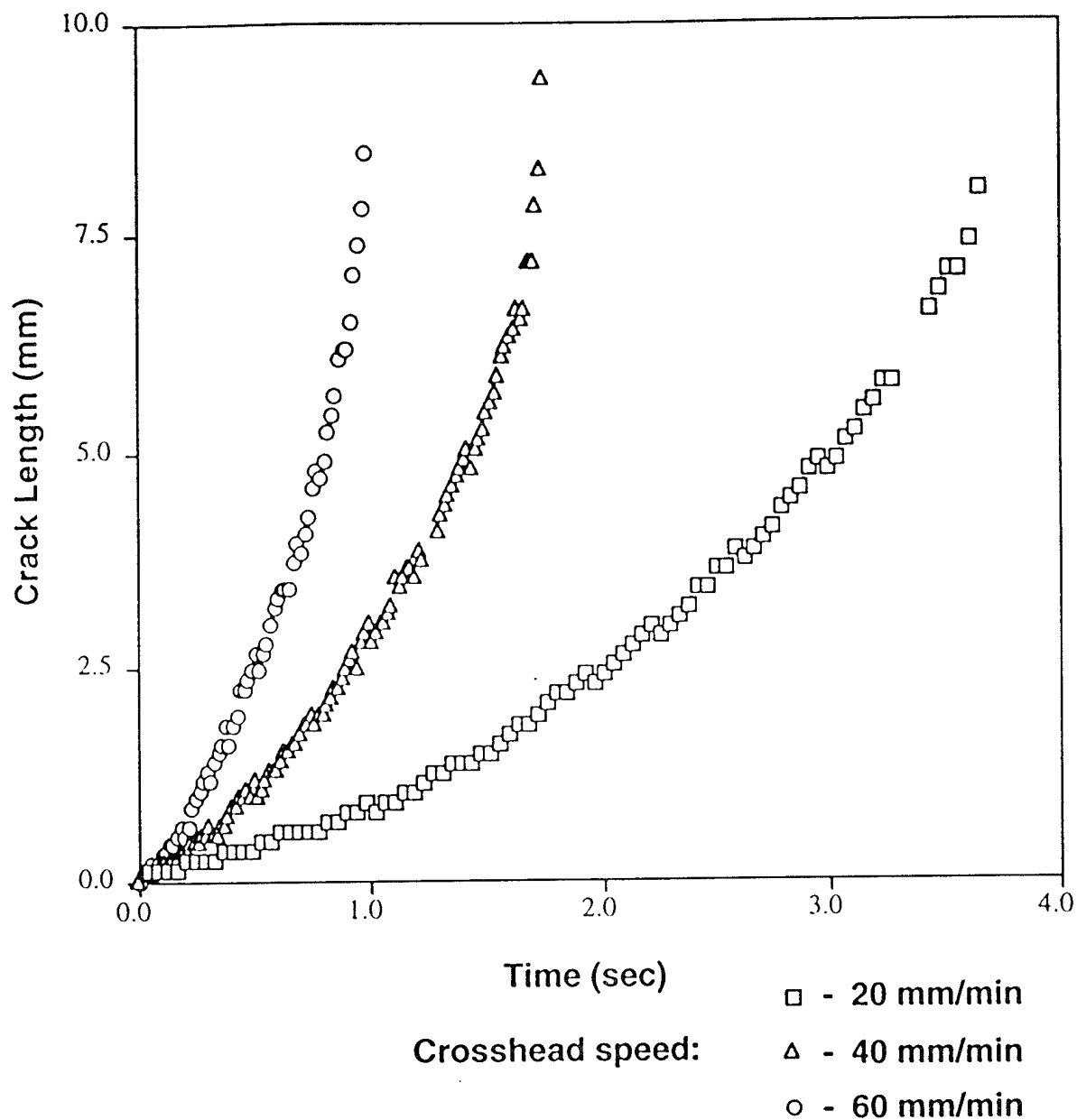
Fig. 6   Plots of the crack length as a function of time, for three different pulling speeds, using the apparatus of Fig. 2.   The crack length measurements were taken from the positions of the higgest temperature pixels in the sequence of stored images.

Together with Dr. Henk van Oene of the Polymer Science Department of the Ford Scientific Research Laboratory, we have recently analyzed these crack initiation and propagation results in terms of the theory of Levy and Herrmann[1]. For an arbitrary load, P, one can write

[1] C. Levy and G. Herrmann, *Eng. Fract. Mech.* 17, 125 (1983).

ON MECHANICAL PROPERTIES OF MATERIALS BY THERMAL WAVE IMAGING

R.L. Thomas, L.D. Favro, and P.K. Kuo, Wayne State University

$$Gda = \frac{P^2 dC}{2}, \tag{1}$$

where G is the energy release rate per unit crack length; $a = 1 + b$, where 1 is the crack length, and b is the notch depth. If we let C be the compliance of the beam, it can be written as

$$C = \frac{2\alpha}{E}, \tag{2}$$

where E is the tensile modulus and α is a function of $\xi = a/h$, and h is the width of the beam. According to this theory, for $a/h < 0.6$, the function, α, is given by the tenth-order polynomial

$$\alpha = 1.98\,\xi^2 - 0.54\,\xi^3 + 18.65\,\xi^4 - 33.7\,\xi^5 + 99.26\,\xi^6 - 211.9\,\xi^7 + 436.84\,\xi^8 - 460.77\,\xi^9 - 289.98\,\xi^{10}. \tag{3}$$

Taking into account that the energy release rate can also be expressed in terms of the fracture toughness, K,

$$G = \frac{K^2}{E}, \tag{4}$$

one sees from Eq. (1) that

$$K^2 = \frac{P^2}{h} \frac{d\alpha}{d\xi}. \tag{5}$$

The testing is carried out at a constant rate of extension. For a given extension, δ, we have

$$\delta = CP. \tag{6}$$

Hence,

$$\frac{d\delta}{dt} = \left[C\frac{dP}{da} + P\frac{dC}{da} \right] \frac{da}{dt}. \tag{7}$$

Since the rate of extension is held constant during the experiment, on may derive an expression for E:

ON MECHANICAL PROPERTIES OF MATERIALS BY THERMAL WAVE IMAGING
R.L. Thomas, L.D. Favro, and P.K. Kuo, Wayne State University

$$E = 2\left[\frac{\alpha}{\alpha_f}\frac{dP}{d(\alpha/\alpha_f)} + \frac{P}{h}\frac{d\alpha}{d\xi}\right]\frac{da/dt}{d\delta/dt}$$

(8)

A "dynamic" energy release rate can now be defined as

$$G_{dynamic} = \frac{K^2}{E}$$

(9)

where K^2 is calculated from Eq. (5) and E is calculated from Eq. (8), once the crack velocity, da/dt, is known. Even though the crack velocity could be calculated from the data, as incremental growth divided by the frame time, this procedure will yield unsatisfactory results, since, intitially, the the crack velocity is very slow and the data set is sufficiently dense that the incremental crack advance contitutes a distance of 0,1, or 2 pixels. Instead, the crack tip location, as revealed by the pixel with the largest increase in temperature, is fitted to an expression for the crack velocity which has been proposed by M.L. Williams[2]

$$\sqrt{\frac{1}{b}+1} + \sqrt{\frac{1}{b}} = \exp(At)$$

(10)

from which the crack velocity can be calculated as:

$$\frac{dl}{dt} = bA\sqrt{\frac{1}{b}+1}\sqrt{\frac{1}{b}}$$

(11)

From a plot of the left side of Eq. (10) as a function of time, one can determine the value of the contant A at different pulling speeds. An example of plots such as this is shown in Fig. 7.

---

[2] M.L. Williams, "The Fracture of a Viscoelastic Material" in Fracture of Metal Solids, Metallurgical Society Conferences, Vol. 20, D.C. Drucker and J.J. Gilman (Eds.), Interscience Publishers, New York (1963).
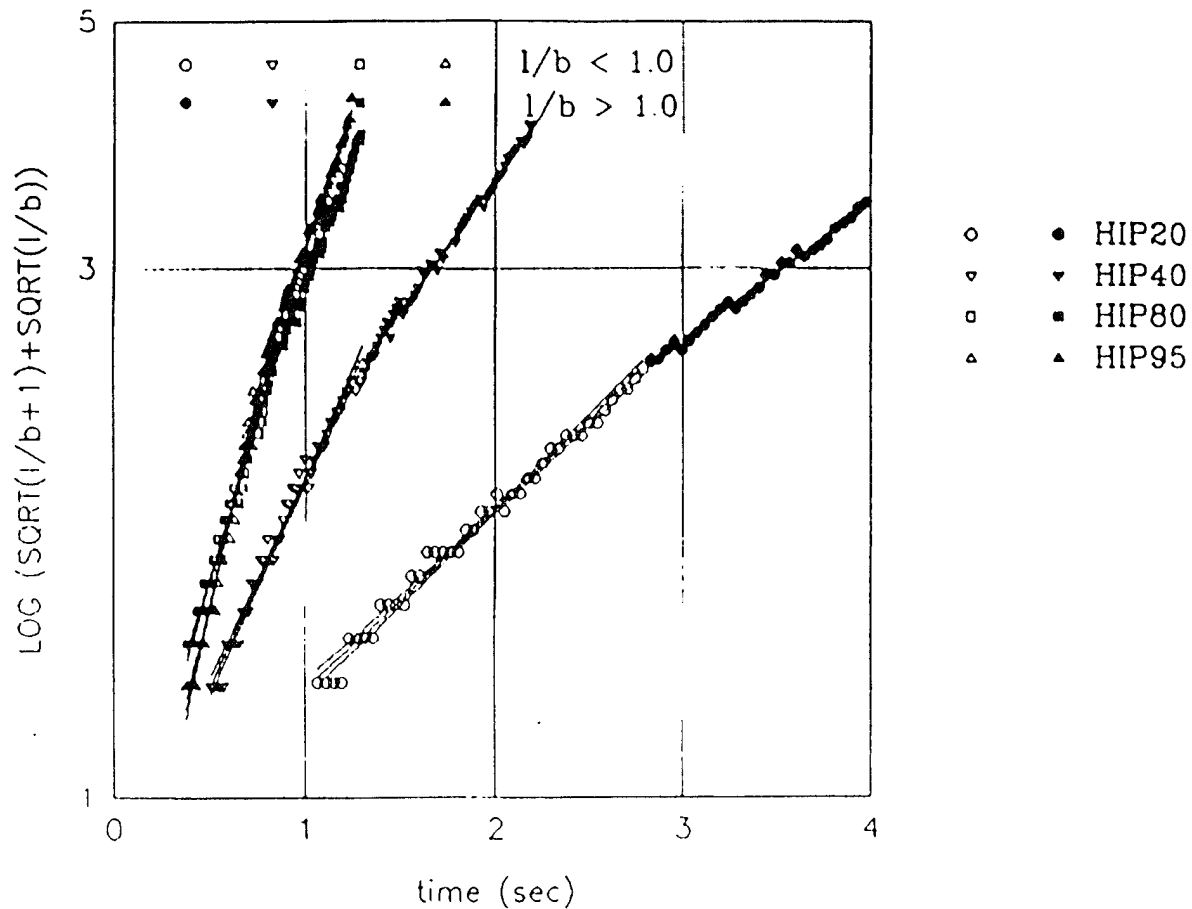
Fig. 7   Plots of the log of the left side of Eq. (10) as a function of time. These plots can be used to determine the constant A in Eqs. (10) and (11).

The values of the contant A determined from Fig. 7 can then be inserted in Eq. (11) to obtain a series of plots of the crack velocity as a function of crack length. The universality of Eq. (10) can be seen in Fig. 8, which plots l/b versus *reduced* time, At. It seen from Fig. 8 that all of the data for l/b > 1 fall on such a universal curve. Plots of the crack velocity versus crack length from Eq. (11), using these values of the constants A, are shown in Fig. 9.
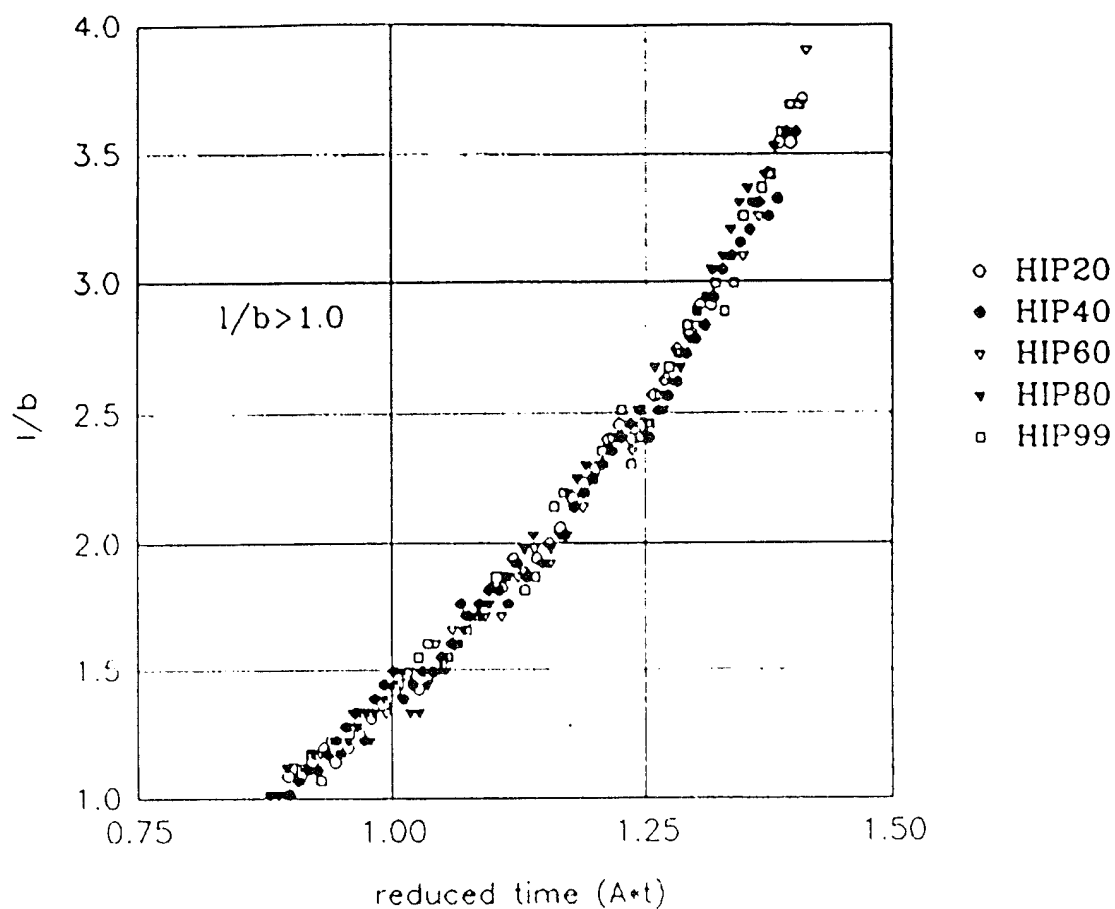
Fig. 8   Plots of 1/b as a function of *reduced* time, At. The fact that all of the plots fit on a single curve demonstrates the universality of Eq. (10).

ALL DATA
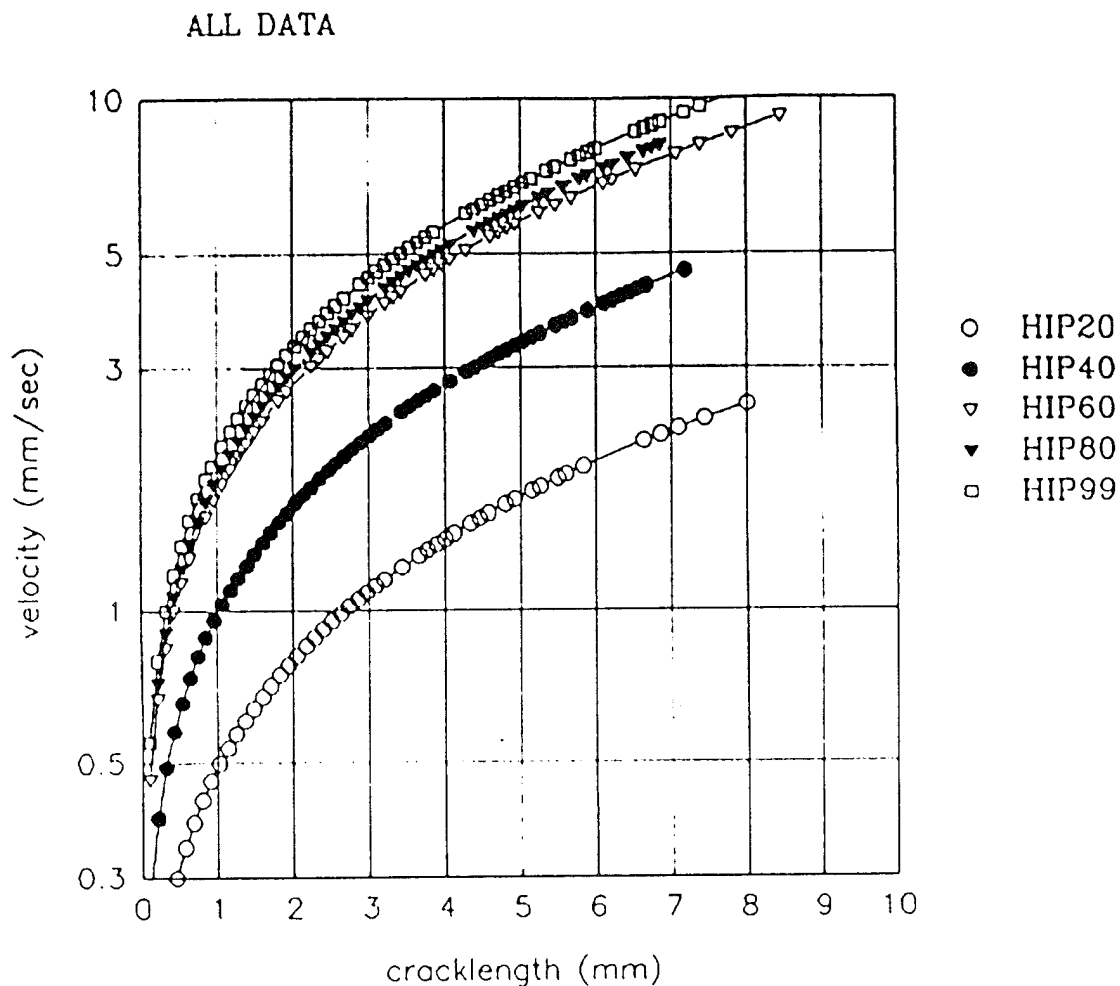
Fig. 9   Plots of the crack velocity as a function of crack length, using the values of the constant A determined from Fig. 7 and Eq. (10).

In Fig. 10, we present plots of the maximum temperature at the crack tip, as a function of time, for five different pulling speeds, using the apparatus of Fig. 2. The temperature measurements were taken from the values of the highest temperature pixels in the sequence of stored images. It is interesting to note that the temperature rise tends to saturate after an initial rapid rise.

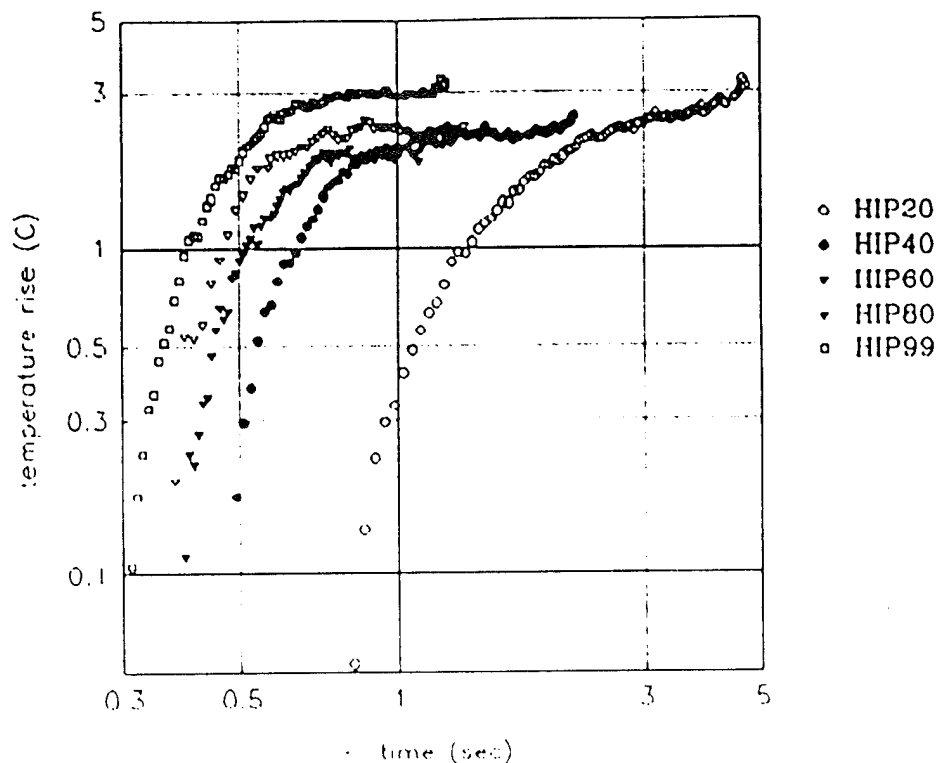Fig. 10   Plots of the maximum temperature at the crack tip, as a function of time, for five different pulling speeds, using the apparatus of Fig. 2. The temperature measurements were taken from the values of the highest temperature pixels in the sequence of stored images.

In addition to the experiments on single-notched coupons, described above, we have also imaged some double-notched coupons to study the interaction between two propagating cracks, and single-notched coupons with defects to study the interaction of propagating cracks with defects. In Fig. 11, we show a sequence of images for a double-notched coupon of high-impact polystyrene, which show adiabatic cooling during elastic deformation, followed by crack tip initiation and plastic deformation, propagation of the two cracks, and the interaction of the two crack tips prior to fracture. The fact that the two crack tips are seen to "repel" one another is quite characteristic, and relates to the stress relief in the plastic deformation zone surrounding each crack.
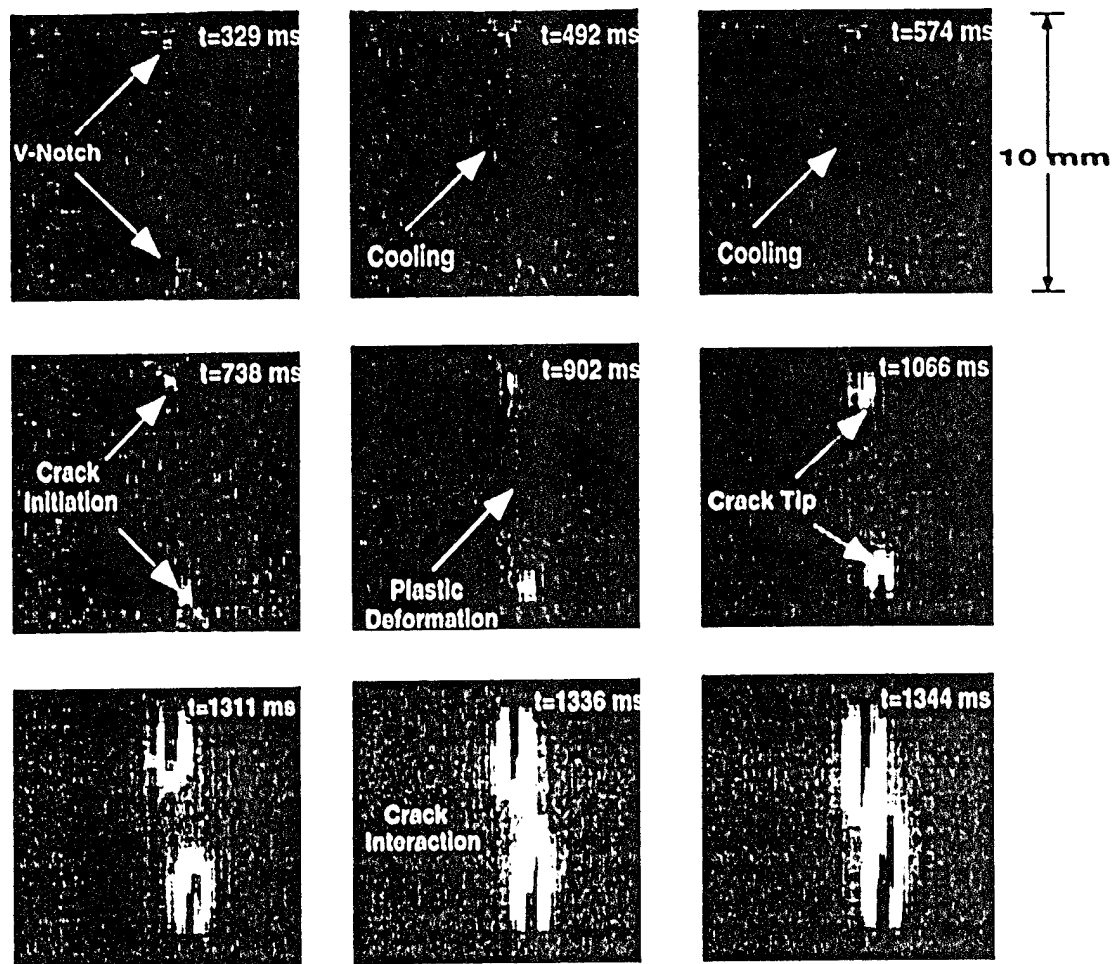
Fig. 11   Sequence of images for a double-notched coupon of high-impact polystyrene, which show adiabatic cooling during elastic deformation, followed by crack tip initiation and plastic deformation, propagation of the two cracks, and the interaction of the two crack tips prior to fracture. The fact that the two crack tips are seen to "repel" one another is quite characteristic, and relates to the stress relief in the plastic deformation zone surrounding each crack.

In Fig. 12, we show a sequence of images for a single-notched coupon of polycarbonate, containing a defect in the form of a bubble. The high elastic stress region, both at the tip of the notch, and around the bubble are seen first to cool, and then to heat as the plastic deformation sets in. While the plastic deformation region passes through the bubble, the crack does not. This behavior is consistent with that seen for the double-notched example of Fig. 11, showing that cracks "avoid" regions in which the stress has been relieved.
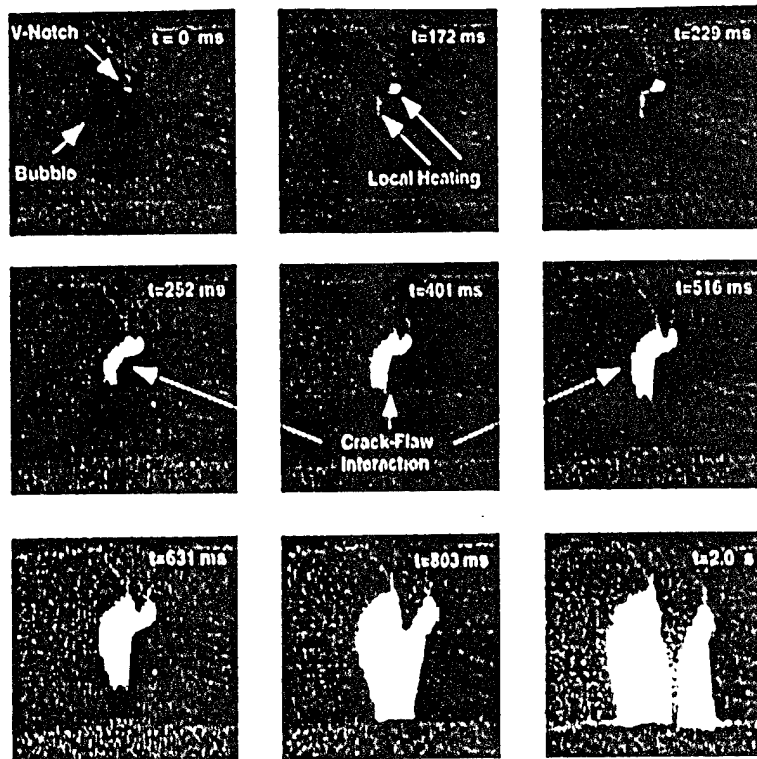
Fig. 12   Sequence of images for a single-notched coupon of polycarbonate, containing a defect in the form of a bubble. The high elastic stress region, both at the tip of the notch, and around the bubble are seen first to cool, and then to heat as the plastic deformation sets in. While the plastic deformation region passes through the bubble, the crack does not. This behavior is consistent with that seen for the double-notched example of Fig. 11, showing that cracks "avoid" regions in which the stress has been relieved.

3)   Thermal Wave Imaging of the Fracture of adhesive joints.

The third topic for which we present important results is that of fracture in adhesive bonds.   In Fig. 13, we show four images of a lap joint between two metal plates, viewed from the side of the joint, as the joint undergoes tensile stress to failure.   It can be seen that cracks intiate at both ends of the joint and propagate towards the center, with a large energy release as the final fracture of the joint. This work was carried out in collaboration with Mr. A.C. Ramamurthy of Ford.   A somewhat different adhesive fracture experiment was carried out in collaboration with Dr. Ray Dickie, also of Ford.   Some of this more recent work has been carried out with a faster frame rate (1 kHz) IR Camera. .   An experimental arrangement for imaging such fracture events is shown in Fig. 14.
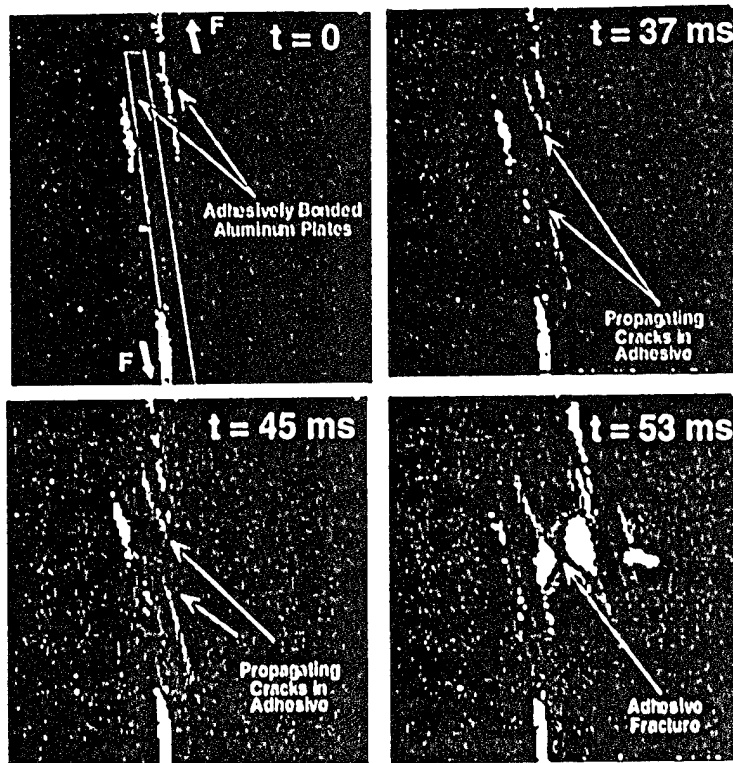
Fig. 13   Sequence of four images of a lap joint between two metal plates, viewed from the side of the joint, as the joint undergoes tensile stress to failure. It can be seen that cracks intiate at both ends of the joint and propagate towards the center, with a large energy release as the final fracture of the joint.

Experimental Setup for Studying Propagating Cracks in Adhesively Bonded Metal Plates
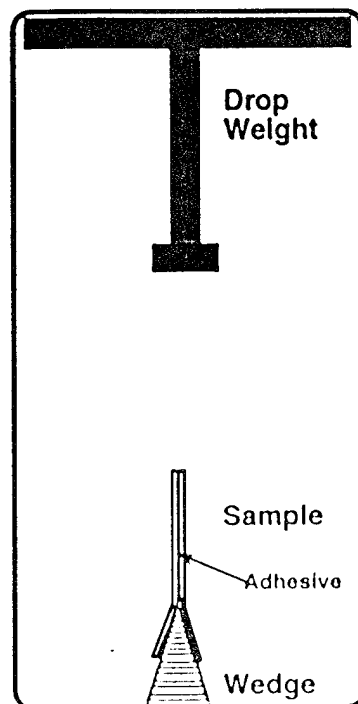

Fig. 14   Experimental setup for studying propagating cracks in adhesively bonded metal plates.   A fast IR camera images the joint from the edge, focussed just above the tip of the wedge where the crack in the adhesive initiates and propagates.
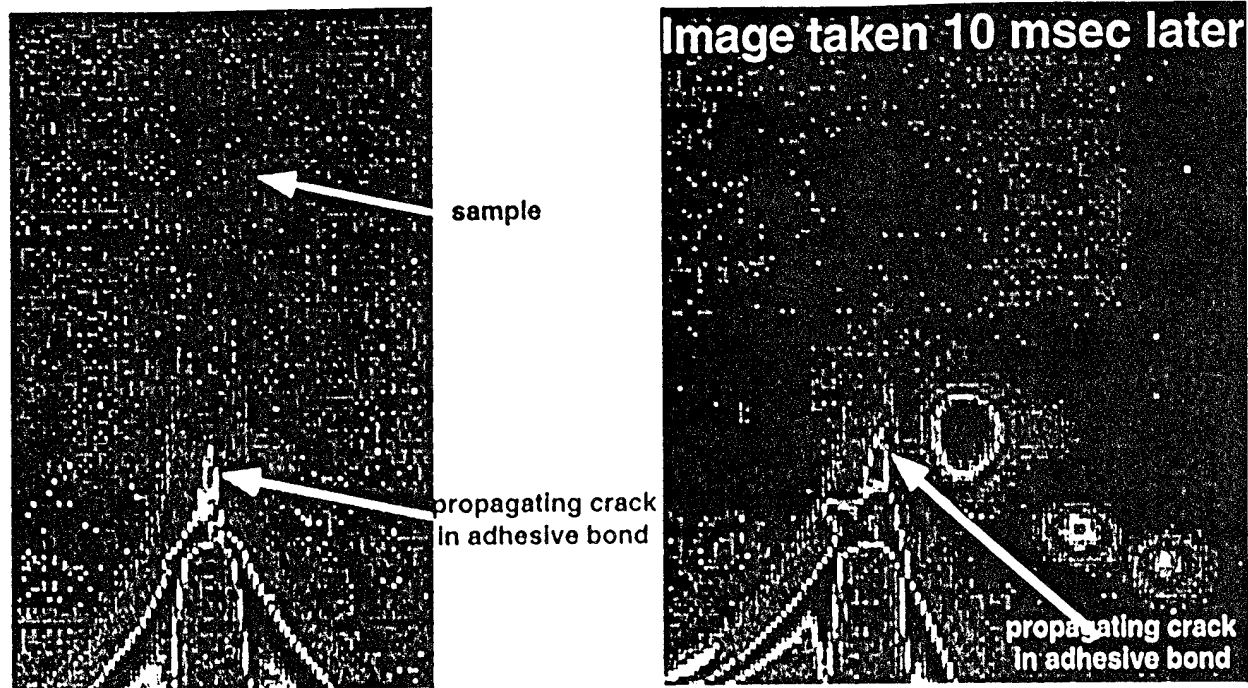
Fig. 15   Two images, taken 10 msec apart, of the propagation of a crack in a metal/metal adhesive bond, using the experimental setup shown in Fig. 14. The total time from initiation of the crack to fracture was 18 msec.

We have recently acquired, through an NSF Instrumentation Grant, combined with University and Industry cost-sharing, a 512 x 512 InSb focal plane array camera, with unique windowing and high frame rate capability. The frame rate for the full array is up to 72 Hz. In addition, there are eight mouse-selectable windows, with higher frame rates, up to 34 kHz. Furthermore, the array operates in a "snapshot" mode - a feature of importance for simplifying the analysis of the time-dependence for various features in the image field. We have also recently acquired a new tabletop tensile tester, with a temperature-controlled sample cell and IR-transparent window, which will permit us to extend the measurements described to temperatures other than room temperature. We are also using this camera to continue our lock-in imaging experiments on semiconductors.

Wayne State University patents and other intellectual property in the area of Thermal Wave Imaging (supported in part by ARO), are currently undergoing technology transfer by a start-up company: Thermal Wave Imaging, Inc. (TWI), 18899 West Twelve Mile Rd., Lathrup Village, MI 48076 [Phone: (810) 569-4960; FAX: (810) 569-4252]. TWI was formed to license from WSU and commercialize patents held by WSU in the area of thermal wave imaging. This technology transfer activity has led to the EchoTherm image acquisition hardware and software (for IBM-PC compatible computers), which it is currently offering for sale. TWI is also engaged in consulting activities for companies interested in applying this existing thermal wave imaging technology to their proprietary NDE problems.

C.   LIST OF ALL PUBLICATIONS AND TECHNICAL REPORTS

"The Thermal conductivity of Isotopically Modified Single Crystal Diamond," Lanhua Wei, P.K. Kuo, R.L. Thomas, T.R. Anthony and W.F. Banholzer, Phys. Rev. Letters 70, No. 24, pp. 3764-3767 (14June, 1993).

"Using Thermal Wave Imaging to See Below the Surface," R.L. Thomas, L.D. Favro, P.K. Kuo and R.Bruno, Photonics Spectra, January, 1993 issue, pp. 148-150.

"Thermal Wave Imaging of the Temperature Distributions around Propagating Cracks in Polymers", R.L. Thomas, L.D. Favro, P.K. Kuo, Z.L. Wu, T. Ahmed, X. Wang, Yingxia Wang, L.C. Jiang, and H. Van Oene Review of Progress in Quantitative NDE, Vol.13, edited by D.O. Thompson and D. Chimenti, Plenum New York, pp. 1641-1644 (1994).

"Thermal Wave Imaging of Propagating Cracks in Polymers," R.L. Thomas, L.D. Favro, P.K. Kuo, Z.L. Wu, T. Ahmed, X. Wang, Yingxia Wang, L.C. Jiang, and H. van Oene, presented at the 8th Int. Topical Meeting on Photoacoustic and Photothermal Phenomena, Pointe-a-Pitre, Guadeloupe (France), January 22-26, 1994, Photoacoustic and Photothermal Phenomena IV, D. Fournier (Ed.) Journal de Physique - Colloques C7 , C7-595-C7-598, 1994.

"Thermal-Wave Imaging of Composites and Polymers," L.D. Favro, P.K. Kuo, and R.L. Thomas, Proc.SPIE Thermosense XVI, Orlando, FL, April 12-16, 1993, Vol 2245, pp. 90-94 (1994).

"High-Speed Infrared Imaging of Fracture in Thermoplastic Olefins," Yingxia Wang, S. Telenkov, Z.L. Wu, T. Ahmed, Xun Wang, L.D. Favro, P.K. Kuo, R.L. Thomas, A.C. Ramamurthy, Witold Brostow, Nankika Anne D'Douza and Henryk Galina, Proc. Adhesion Society Meeting: January, 1995, Dayton TX.

D.   LIST OF ALL PARTICIPATING SCIENTIFIC PERSONNEL SHOWING ANY ADVANCED DEGREES EARNED BY THEM WHILE EMPLOYED ON THE PROJECT

Prof. R.L. Thomas

Prof. L.D. Favro

Prof. P.K. Kuo

Dr. Tasdiq Ahmed (Postdoctoral Research Associate)

Dr. David Crowther (Postdoctoral Research Associate)

Z.J. Feng (visiting scholar)

Huijia Jin (visiting scholar)

Yang Chen (GRA)

Xiaoyan Han (GRA)

Yuesheng Lu (GRA)

Yingxia Wang (GRA)

Xun Wang (GRA)